Entanglement entropy of a three-spin-interacting spin chain with a time-reversal-breaking impurity at one boundary

Tanay Nag[1] and Atanu Rajak[2]
[1]*Max Planck Institute for the Physics of Complex Systems, Nöthnitzer Str. 38, Dresden 01187, Germany*
[2]*Department of Physics, Jack and Pearl Resnick Institute, Bar-Ilan University, Ramat-Gan 52900, Israel*

(Received 14 November 2017; published 9 April 2018)

We investigate the effect of a time-reversal-breaking impurity term (of strength λ_d) on both the equilibrium and nonequilibrium critical properties of entanglement entropy (EE) in a three-spin-interacting transverse Ising model, which can be mapped to a p-wave superconducting chain with next-nearest-neighbor hopping and interaction. Importantly, we find that the logarithmic scaling of the EE with block size remains unaffected by the application of the impurity term, although, the coefficient (i.e., central charge) varies logarithmically with the impurity strength for a lower range of λ_d and eventually saturates with an exponential damping factor [$\sim \exp(-\lambda_d)$] for the phase boundaries shared with the phase containing two Majorana edge modes. On the other hand, it receives a linear correction in term of λ_d for an another phase boundary. Finally, we focus to study the effect of the impurity in the time evolution of the EE for the critical quenching case where the impurity term is applied only to the final Hamiltonian. Interestingly, it has been shown that for all the phase boundaries, contrary to the equilibrium case, the saturation value of the EE increases logarithmically with the strength of impurity in a certain regime of λ_d and finally, for higher values of λ_d, it increases very slowly dictated by an exponential damping factor. The impurity-induced behavior of EE might bear some deep underlying connection to thermalization.

DOI: 10.1103/PhysRevE.97.042108

I. INTRODUCTION

Study of various quantum information theoretic measures, such as fidelity [1], decoherence [2,3], concurrence [4,5], quantum discord [6], and entanglement entropy (EE) [7], has grabbed immense attention as it connects the quantum information science [8–14], statistical physics, and condensed matter physics [15–18] in a concrete way. All of the above quantities are able to capture the ground-state singularity and thus are used as indicators of quantum phase transition (QPT). For example, the EE of a block of length l quantified by von Neumann entropy is given by

$$S(l) = -\mathrm{Tr}(\rho_l \ln \rho_l), \tag{1}$$

where the reduced density matrix $\rho_l = \mathrm{Tr}_{L-l}(\rho)$ is obtained after tracing over the block of length $L - l$ from the composite system of length L with pure state density matrix ρ. For a one-dimensional homogeneous critical spin chain with open boundary conditions, the EE scales with the shortest length scale (l) of the system as $S = \frac{c}{6} \ln l + \gamma$, where c is a universal quantity and given by the central charge of the underlying conformal field theory, whereas γ is a nonuniversal constant [7,19]. In the context of disordered spin chain (i.e., inhomogeneous case), for the critical case, it has been shown that the EE still varies logarithmically with block size but it acquires an effective central charge different from the bare central charge derived in the clean limit [20]. It has been shown that the effective central charge also appears for the interface defects in a spin chain [21].

At the same time, the study of entanglement spectrum and EE in quantum many-body systems has initiated a plethora of intensive research to characterize a topological system, through the concept of quantum entanglement [22–26]. The topological phases are characterized by a topological invariant number (Chern number or Z_2 invariant or zero-energy Majorana modes) and this phase supports edge modes [27,28]. In the connection of EE and edge state, it is noteworthy that the equilibrium EE receives a finite contribution from the localized boundary states in addition to the contribution from the bulk energy spectrum. The finite contribution from boundaries is associated to the nonzero value of the Berry phase [29]. A nonextensive correction to the area law of EE, named as topological EE, has been proposed as a tool to characterize the topological phases of the system [30]. Interestingly, it has been shown for a two-dimensional spin-orbit coupled superconductor that the derivatives of the EE with respect to model parameters are sharply peaked at the point of topological phase transitions [31].

In parallel, the behavior of the EE in quantum systems considering a nonequilibrium situation has received an enormous amount of attention in recent years [32–38]. The upsurge of such studies is motivated by the experimental demonstration in optical lattice [39]. In particular, an out-of-equilibrium one-dimensional Bose gases has been prepared experimentally using the combination of a two-dimensional optical lattice and a crossed dipole trap [40,41]. It has been shown that a global sudden quench leads to an initial linear rise of the EE with time followed by a saturation [32]. Moreover, the dynamics of EE in the random transverse-field Ising chain after a sudden critical quench becomes ultraslow and has a double-logarithmic time dependence [42]. Also, the robustness of the Majorana zero mode in the infinite time limit following a sudden quench of a one-dimensional p-wave superconductor has been investigated by examining the one-particle

entanglement spectrum [43]. The quench dynamics in optical lattice with Rb^{87} atoms is experimentally investigated in the context of quantum information namely, the signature of Lieb-Robinson bound of light-cone-like spreading of correlations is studied [44]. Moreover, optical interferometry is directly used to measure entanglement entropy in a quantum many-body system composed of ultracold bosonic atoms in optical lattices [45].

In recent years, a considerable amount of work has been carried out to investigate the topological properties of one-dimensional p-wave Majorana chain [46–56]. Our main aim here is to study the effect of a single impurity, located at one of the boundaries, on the critical behavior of the EE in this model with an additional next-nearest-neighbor hopping term. This single impurity indeed breaks the time-reversal invariance of the system. We show that in the equilibrium case, the derivative of EE can be used as an indicator of QPTs. We find that the scaling relation of the EE with the subsystem size remains same as obtained in the inhomogeneous case with an effective central charge. This effective central charge here shows a logarithmic scaling relation with λ_d for an initial window of λ_d and eventually saturates for large value of λ_d. This phenomena is observed at the phase boundaries shared with the phase containing two Majorana modes sitting at each end of the chain. On the other hand, for the phase boundary separating topological phase with one Majorana mode from nontopological one, the effective central charge acquires a linear correction due to this impurity term. Additionally, for the nonequilibrium time evolution of EE obtained by adding a boundary impurity term to the critical quenched chain, irrespective of the nature of phase boundaries the logarithmic behavior and the subsequent exponential scaling show up only in the saturation value of the EE but not in the initial rise of EE.

This paper is organized as follows. In Sec. II we introduce the three-spin-interacting transverse field Ising model and discuss its phase diagram. We also mention the effect of an impurity term on the different phases of the model. In Sec. III, we present the method to compute EE and extend it to calculate the time evolution of the EE numerically. In Sec. IV, we illustrate our results for equilibrium as well as for nonequilibrium case. Finally, we provide our concluding remarks in Sec. V.

II. MODEL

The Hamiltonian we consider here is given by a three-spin-interacting transverse Ising model with N spins [57]

$$H = -\sum_n \left(h\sigma_n^z + \lambda_1\sigma_n^x\sigma_{n+1}^x + \lambda_2\sigma_{n-1}^x\sigma_n^z\sigma_{n+1}^x\right), \quad (2)$$

where h, λ_1, and λ_2 are transverse magnetic field, cooperative interaction and three-spin interaction, respectively, and, σ^α ($\alpha = x,y,z$) are the standard Pauli matrices. Using Jordan-Wigner transformation the model can be written in terms of spinless fermions with a next-nearest-neighbor hopping and superconducting pairing terms. At the same time, one can rewrite the Hamiltonian in terms of Majorana fermions with

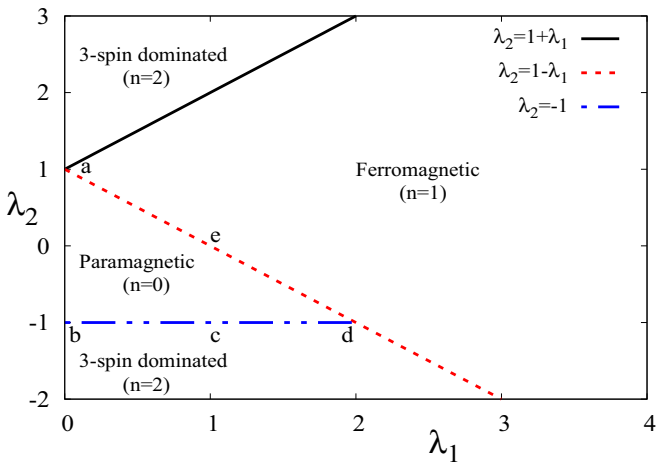

FIG. 1. Zero-temperature phase diagram of the model Hamiltonian (2) for $h = 1$. The line $\lambda_2 = 1 + \lambda_1$ represents the phase boundary between upper three-spin dominated phase (with two zero-energy Majorana end modes at each edge) and ferromagnetic phase with one Majorana at each end. There are two more phase boundaries, given by $\lambda_2 = 1 - \lambda_1$ (a-e-d line) and $\lambda_2 = -1$ (b-d line). The paramagnetic region denoted by $n = 0$ does not have any zero-energy Majorana mode. In terms of topology both the three-spin dominated phases have two zero-energy Majorana modes at each end.

open boundary condition (OBC), given by

$$H = -i\left[-h\sum_{n=1}^{N} b_n a_n + \lambda_1 \sum_{n=1}^{N-1} b_n a_{n+1} + \lambda_2 \sum_{n=2}^{N-1} b_{n-1} a_{n+1}\right], \quad (3)$$

where, $a_n = c_n^\dagger + c_n, b_n = -i(c_n^\dagger - c_n)$ are Majorana fermions. The system discussed above has time-reversal symmetry ($T^2 = 1$). This transformation T is defined as the complex conjugation of all the objects in the Hamiltonian (3). As a result, T leads to $a_n \to a_n$ and $b_n \to -b_n$, and hence, Eq. (3) is invariant under time reversal [53].

We now briefly discuss the phase diagram of the model with $h = 1$ (see Fig. 1). This model has three phases: (i) the ferromagnetic phase, which is topologically nontrivial hosting one unpaired Majorana at each end, i.e., a_1 and b_N; (ii) the paramagnetic phase, a nontopological phase, with no Majorana edge modes; and (iii) three-spin-dominated topological phase with two unpaired Majorana modes at each edge, i.e., a_1 and a_2 are at the left boundary with b_N and b_{N-1} exist at the right boundary. The details of the model and phase diagram are discussed in Refs. [58,59].

It is noteworthy that a similar kind of model, namely, cluster-Ising model, has been studied before in the context of locating its QPTs between cluster and antiferromagnetic phases using geometric [60] and multipartite [61] entanglement. Although, the three-spin-dominated phase of the model (2) is analogous to the cluster phase of the cluster-Ising model, there are a few differences between these two models: (i) model given in Eq. (2) contains an extra transverse field term; (ii) it has Z_2^T symmetry (an antiunitary Z_2 symmetry, $\sigma_x \to -\sigma_x$) [62], whereas the cluster-Ising model is symmetric under is symmetric under $Z_2 \times Z_2$; and (iii) the dual model of (2) is a

transverse XY spin chain, on the other hand, the cluster-Ising model is its self-dual.

Our main goal is to find the effect of an impurity term in the critical behavior of the EE for both equilibrium and nonequilibrium cases. To achieve this goal, we introduce an additional term in the Hamiltonian (3) of the form [59]

$$H_{\rm imp} = -i\lambda_d a_j a_q, q = j + m. \tag{4}$$

The impurity term (4) affects the phase with two Majorana modes at one end (three-spin-dominated phase). We here take into account the impurity term (4), located in the left edge of the system, that results in the annihilation of the a-type Majorana modes, however, the b-type Majorana modes residing at the right edge remain intact [58,59]. In contrast, the phase with one Majorana mode at each end remains unaffected. This term breaks the time-reversal symmetry of the system as T reverses the sign of $H_{\rm imp}$. The annihilation of the edge Majorana mode is related to this symmetry breaking.

In the spin representation, the impurity Hamiltonian is expressed as $H_{\rm imp} = \lambda_d \sigma_j^y \prod_{n=j+1}^{j+m-1}(-\sigma_n^z)\sigma_{j+m}^x$, which is a string operator. Therefore, in the spin language, the breaking of time-reversal symmetry of the model in Eq. (3) is related to the breaking of Z_2^T symmetry as the impurity term explicitly breaks this symmetry. Similarly for the cluster-Ising model, we note that if one considers an additional impurity term, breaking $Z_2 \times Z_2$ symmetry of the cluster phase, the existence of the edge Majorana modes might get affected in a similar fashion there also.

As mentioned already, the impurity term is a nonlocal string operator, though, in the Majorana language we can say it is quasilocal [see Eq. (4)]. We hence stress that the impurity is purely quantum in nature. In parallel, the effect of a classical impurity, the zero transverse field at the first site of an otherwise homogeneous chain, has been investigated in a quantum Ising chain by studying the finite-size scaling of the magnetizations [63]. The nature of this impurity is classical due to the fact that the leftmost spin can not flip; in contrast, the impurity term considered in Eq. (4) is able to flip the spins. Simultaneously, transverse Ising model with multi-impurities gives rise to many nontrivial changes in deformation energy and specific heat [64].

Connecting to experimental realization, the impurity term in Eq. (4) can be prepared by experiments on entangled atoms in optical lattice. The array of parallel spin chains are created from two-dimensional degenerate gas of ^{87}Rb atoms by applying two horizontal optical lattice beams. The atoms are initially prepared in a hyperfine state and then impurity is introduced by changing the hyperfine structure of one of the atoms [65].

III. ENTANGLEMENT ENTROPY

We will here present our numerical method to calculate EE in the Majorana basis under the sudden quenching of a parameter of the chain. In order to formulate the nonequilibrium EE, we first briefly discuss the equilibrium EE in the Majorana basis [66]. Let us consider a general quadratic form of Eq. (3) in terms of Majorana operators

$$H = \frac{i}{4}\sum_{m,n=1}^{2N} e_m A_{mn} e_n, \tag{5}$$

where $e_{2m-1} = a_m$ and $e_{2m} = b_m$. The matrix elements for A are given by $A_{n,n+1} = -A_{n+1,n} = 1$, $A_{2n,2n+1} = -A_{2n+1,2n} = -\lambda_1$ and $A_{2n,2n+3} = -A_{2n+3,2n} = -\lambda_2$. The impurity Hamiltonian (4) generates two extra elements in the matrix A: $A_{2j-1,2j+2m-1} = -A_{2j+2m-1,2j-1} = -\lambda_d$.

Let $W \in SO(2N)$ be a special orthogonal matrix that makes A block diagonal of the form,

$$D = \bigoplus_{k=1}^{N} \tilde{\epsilon}_k \begin{bmatrix} 0 & 1 \\ -1 & 0 \end{bmatrix}, \tag{6}$$

where $D = WAW^\dagger$. Now, a new set of Majorana operators is defined as

$$d_p = \sum_{m=1}^{2N} W_{pm} e_m, \quad \text{where} \quad p = 1, \ldots, 2N. \tag{7}$$

Here, d_p satisfies the relations $d_p^\dagger = d_p, \{d_p, d_q\} = 2\delta_{pq}$ The Hamiltonian in Eq. (5) in terms of the new Majorana operators is given by

$$H = \frac{i}{4}\sum_{k=1}^{N} \tilde{\epsilon}_k (d_{2k-1} d_{2k} - d_{2k} d_{2k-1}). \tag{8}$$

We can now define the ground-state correlation matrix $\langle d_p d_q \rangle = \delta_{pq} + i\Gamma^B_{pq}$ where Γ^B is given by

$$\Gamma^B = \bigoplus_{k=1}^{N} \begin{bmatrix} 0 & 1 \\ -1 & 0 \end{bmatrix}. \tag{9}$$

Finally, we obtain the correlation matrix $\langle e_m e_n \rangle = \delta_{mn} + i\Gamma^A_{mn}$ in terms of initial Majorana operators e. The matrix Γ^A is found from Γ^B using the relation

$$\Gamma^A = W^\dagger \Gamma^B W. \tag{10}$$

As shown in Appendix A, the EE for a block of length l is given by

$$S(l) = -\sum_{n=1}^{l} \left[\left(\frac{1+\eta_n}{2} \right) \log \left(\frac{1+\eta_n}{2} \right) + \left(\frac{1-\eta_n}{2} \right) \log \left(\frac{1-\eta_n}{2} \right) \right], \tag{11}$$

where η_n are the imaginary part of the purely imaginary eigenvalues of the $2l \times 2l$ skew-symmetric matrix Γ^A. We note that the eigenvalues come in pairs.

Now, we will extend the above equilibrium technique for calculating the EE in a situation when the system is suddenly driven out of equilibrium. We consider the Majorana Hamiltonian H that instantaneously changes from $H = H_i$ to $H = H_f$ at time $t = 0$. We therefore have two sets of W, namely, W_i and W_f, which can transform two Hamiltonians H_i and H_f into two block diagonal form as mentioned in Eq. (6). Similar to Eq. (7), we can now define two new set of Majorana

operators corresponding to the Hamiltonians H_i and H_f given by

$$d_p = \sum_{m=1}^{2N} (W_i)_{pm} e_m \quad \text{and} \quad d'_p = \sum_{m=1}^{2N} (W_f)_{pm} e_m. \tag{12}$$

Let us assume that $|\psi_i\rangle$ is the ground state (in the Majorana basis) of the initial Hamiltonian H_i. Using the relation $\langle\psi_i|e_m e_n|\psi_i\rangle = \delta_{mn} + i\Gamma^A_{mn}$, the correlation matrix looks like $\langle\psi_i|d'_p d'_q|\psi_i\rangle = \delta_{pq} + i\Gamma'^B_{pq}$, where $\Gamma'^B = W_f \Gamma^A W_f^\dagger$. The point to note here is that the matrix Γ^A is calculated using the parameters of the initial Hamiltonian H_i given by $\Gamma^A = W_i^\dagger \Gamma^B W_i$ where the expression of Γ^B is shown in Eq. (9). Under the nonequilibrium dynamics, the time dependence of the above-mentioned correlation matrix can be determined as $\langle\psi_i|d'_p(t)d'_q(t)|\psi_i\rangle = \delta_{pq} + i\Gamma'^B_{pq}(t)$ where $\Gamma'^B(t) = \exp(iH_f t)\Gamma'^B \exp(-iH_f t)$. Finally, in order to calculate the time-evolved EE, we compute the time-dependent correlation matrix after a sudden quench given by $\langle\psi_i|e_m(t)e_n(t)|\psi_i\rangle = \delta_{mn} + i\Gamma^A_{mn}(t)$, where

$$[\Gamma^A(t)]_{2l\times 2l} = [W_f^\dagger]_{2l\times 2N}[\Gamma'^B(t)]_{2N\times 2N}[W_f]_{2N\times 2l}. \tag{13}$$

For each time instant the matrix in Eq. (13) is diagonalized and then the EE can be calculated using Eq. (11) as a function of time.

IV. RESULTS

We here investigate the effect of the impurity term $H_{\rm imp} = -i\lambda_d a_1 a_2$ in the critical behavior of EE under both equilibrium and nonequilibrium cases where the $H_{\rm imp}$ is only applied to the final quenched Hamiltonian.

A. Equilibrium

The quantum information theoretic measures such as the fidelity [1], the Loschmidt echo [2,67,68], the quantum discord [69,70], and the entanglement entropy are currently being studied intensively in the context of characterizing QPTs in various condensed matter systems. In this section, we will first show the EE as an indicator of the QPTs of the model (2). We open our study by calculating the derivative of the EE, and plot as a function of λ_2 to get the phase transition points as shown in Fig. 2. The derivative of EE shows dip, peak, or kink at the QCPs. It is noteworthy that the impurity has a noticeable effect on the derivative $\Delta S/\Delta\lambda_2$ over the phase boundaries separating a topological or a nontopological phase from $n = 2$ topological phase, since it destroys two Majorana modes of the left end of the chain. In the inset of Fig. 2, we have plotted the EE as a function of λ_2 for various values of λ_d by fixing $\lambda_1 = 1$. It shows that the peak value of the EE decreases at $n = 2{-}n = 1$ and $n = 2{-}n = 0$ phase boundaries with increasing λ_d, on the other hand, it indeed increases for $n = 1{-}n = 0$ boundary. This feature gets reflected in the derivative where the dip height in $n = 2{-}n = 1$ and $n = 2{-}n = 0$ phase boundaries reduces with λ_d and peak height in $n = 1{-}n = 0$ boundary enhances.

The noteworthy feature observed in the derivative at these phase boundary points is that the peak or dip for $\lambda_d = 0$ changes to dip or peak for any finite λ_d and the height

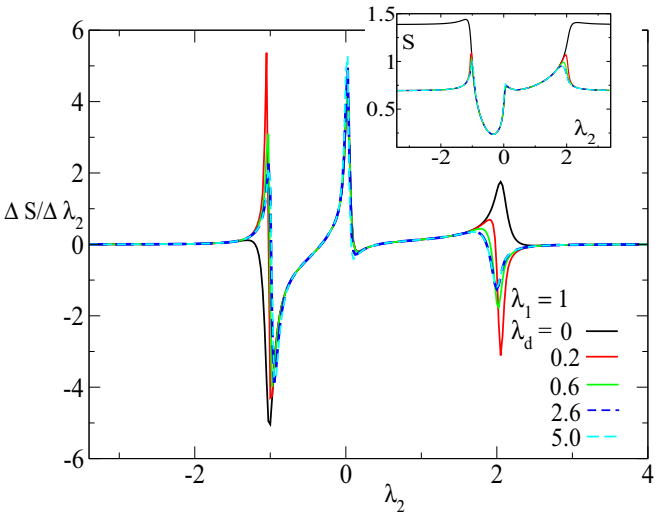

FIG. 2. The derivative of EE with λ_2 shows peak, dip or kink at the phase boundaries pointing toward the fact that it can be used as an indicator of QPTs. For $\lambda_d = 0$, the derivative shows a dip at $n = 2{-}n = 0$ phase boundary while the peaks are observed for $n = 1{-}n = 0$ and $n = 1{-}n = 2$ phase boundaries. These dip and peak in the derivative of EE that appear in the phase boundaries separating $n = 2$ phase with others change to a kink like structure for finite λ_d. This qualitative change in behavior of the derivative is clearly evident from the variation of EE with λ_2 as shown in the inset (we set $\lambda_1 = 1$); the value of EE reduces inside the $n = 2$ phase when λ_d becomes finite. The dip or peak height of the derivative at these kinks is maximum for an infinitesimal impurity strength and decreases with increasing λ_d; inset suggests similar feature that at $n = 2{-}n = 0$ and $n = 1{-}n = 2$ phase boundaries the EE shows a peak that decreases with λ_d. In contrast, at $n = 0{-}n = 1$ phase boundary, the peak height of the derivative enhances with λ_d as peak height of EE increases. We choose the system size to be $N = 100$ and block length to be $l = 30$.

associated with them decreases with increasing λ_d. These behavior are observed over the phase boundaries that separates $n = 2$ phase from others. For, $\lambda_d = 0$, the EE decreases when the system enters from $n = 2$ phase to $n = 0$ phase, whereas for finite λ_d, the reverse occurs. Hence, the dip observed in the derivative turns into a peak for a finite λ_d. On the other hand, the peak structure remains unaffected over the $n = 0{-}n = 1$ phase boundary as the impurity term is introduced.

We will now analyze the behavior of EE in three phases extensively as shown in the inset of Fig. 2. For $\lambda_d = 0$, the EE remains almost constant inside lower $n = 2$ phase and then after it starts decreasing around $\lambda_2 = -1$; it reaches minimum value in the $n = 0$ phase. Afterwards it starts increasing up to $\lambda_2 = 2$, in between, showing a kink around $n = 0{-}n = 1$ boundary (where $\lambda_2 = 0$). Finally, it saturates inside the upper $n = 2$ phase to the same value as of the lower one. Furthermore, the value of EE reduces in both the $n = 2$ phases in the presence of the impurity, whereas it remains almost unchanged inside $n = 0$ and $n = 1$ phases.

We can explain this phenomena qualitatively by considering that the EE in Eq. (11) consists three contributions, given by

$$S(l) = S_{BU} + S_B^L + S_B^R, \tag{14}$$

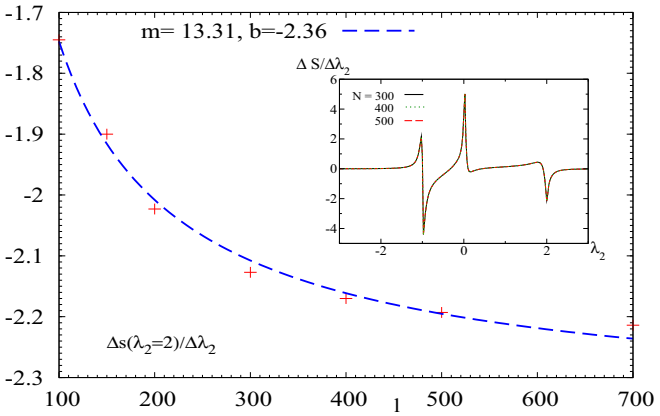

FIG. 3. Plot shows that peak or dip, observed in the derivative of EE for a clean system with $\lambda_d = 0.1$, becomes more sharper with block size l. We choose $n = 1{-}n = 2$ phase boundary. We see that $\frac{\Delta S(\lambda_2=2)}{\Delta\lambda_2}$ matches well with $(m/l)\log l + b$ (depicted by blue dashed lines) where m and b is found to be 13.31 and -2.36. Inset shows the variation of the derivative with l by varying λ_2 and λ_1 is kept fixed at unity.

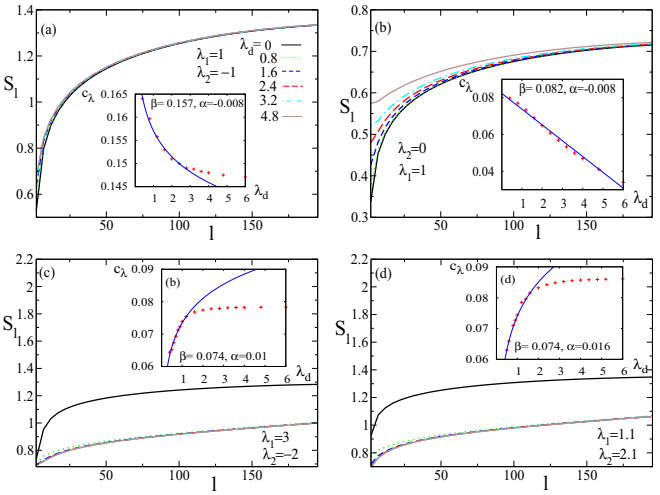

FIG. 4. The equilibrium EE, S_l as function of block length l for different values of λ_d is plotted for (a) $n = 2{-}n = 0$ (with $\lambda_2 = -1$), (b) $n = 1{-}n = 0$ (with $\lambda_2 = 0$), (c) $n = 2{-}n = 1$ (with $\lambda_2 = -2$), and (d) $n = 2{-}n = 1$ (with $\lambda_2 = 2.1$) phase boundaries. For (a) and (b), the EE becomes maximum for $\lambda_d = 4.8$ as shown by the solid brown line appeared at the top of the plots. The dotted long-dashed sky line with $\lambda_d = 3.2$, long-dashed red line with $\lambda_d = 2.4$, short-dashed blue line with $\lambda_d = 1.6$, dotted green line with $\lambda_d = 0.8$, and solid black line with $\lambda_d = 0$ appear in a decreasing order. The order is reversed for (c) and (d) compared to (a) and (b). The value of EE with the impurity strength λ_d increases for (a) and (b), whereas decreases for (c) and (d). The inset shows the variation of the effective central charge c_λ as a function of λ_d. The behavior exhibited by c_λ is opposite to that of the EE in all the above cases. Additionally, insets of (a), (c), and (d) show that c_λ varies logarithmically with λ_d for $\lambda_d^l < \lambda_d < \lambda_d^u$; $c_\lambda = \alpha \log \lambda_d + \beta$ (indicated by blue solid lines). On the other hand, for (b) it is linear throughout the range of λ_d; $c_\lambda = \alpha\lambda_d + \beta$ (drawn using blue solid lines). In this case, β equals to the central charge ($c_0 = 1/12$) for the clean system. Numerically, the extrapolated value of c_λ at $\lambda_d = 0$ is $\beta = c_0 = 0.082$ (close to $1/12$).

where the contributions $S_{\rm BU}$, S_B^L, and S_B^R come from bulk, left, and right boundary modes of the system, respectively. The EE inside the $n = 2$ phases has all three contributions of Eq. (14), since there exists two Majorana modes in each end. On the other hand, the $n = 0$ phase does not host any Majorana edge mode that results only bulk contribution in the EE. Again, since the $n = 1$ phase has one Majorana mode at each end, the EE has all three contributions but the value will be less than that of the $n = 2$ phase. Now, once the impurity term is applied, the constant value of EE obtained for $\lambda_d = 0$ case inside the $n = 2$ phases decreases, but it does not depend on the impurity strength. This is due to the fact that the application of the impurity term, the left end Majorana modes of $n = 2$ phases vanish, although the right end modes remain intact. As a result, the left end modes do not contribute in the EE [see Eq. (14)], which reduces the EE compared to the $\lambda_d = 0$ case. On the other hand, inside $n = 0$ and $n = 1$ phases the EE for $\lambda_d = 0$ and $\neq 0$ coincides with each other. This phenomena can be explained using the fact that the Majorana mode of $n = 1$ phase remains unaffected by the impurity term. Therefore, the EE has all three terms as described in Eq. (14) even after the application of λ_d. As mentioned already, since the $n = 0$ phase does not have any zero mode it remains unaffected by the impurity. This explains the behavior of the EE inside the $n = 0$ and $n = 1$ phases in the presence of the impurity.

In parallel, we investigate the height of the singularities in derivative of the EE as a function of block size l for $\lambda_d = 0.1$. It can be noted that dip or peak in Fig. 3 becomes sharper with increasing block length l. Here we have studied height of dips at $n = 2{-}n = 1$ boundary and found that it varies as $l^{-1}\log l$. Our result for derivative of the EE is in accordance with the study of the finite-size effect of EE in one dimensional topological system [71]. Similar to scaling function associated with free energy [72], here also the finite-size scaling of EE is sensitive to the topological character of the model.

Our aim is now to study the variation of S_l with l for different values of impurity strength over various phase boundaries (see Fig. 4). As mentioned before, the critical EE shows a scaling relation $S_l = c_0 \log l + \gamma$ with the block size l, where $c_0 = c/6$ and c being the central charge and γ is a nonuniversal constant. As shown in Fig. 4, in the presence of the impurity term the EE follows similar scaling relation as in the clean case with an effective c_0 (namely, c_λ) and nonuniversal constant γ_λ, which depend on λ_d: $S_l = c_\lambda \log l + \gamma_\lambda$. The EE on the anisotropic critical line $n = 0{-}n = 2$ is minimally increased by λ_d [see Fig. 4(a)], whereas the EE increases substantially for Ising critical line with $\lambda_2 = 0$ [see Fig. 4(b)]. In contrast, for $n = 1{-}n = 2$ phase boundaries the value of EE reduces considerably compared to $\lambda_d = 0$ once a finite λ_d is applied [see Figs. 4(c) and 4(d)]. However, it does not change so much for two different values of λ_d. We have plotted c_λ, which essentially captures the signatures of the effective central charge, as a function of λ_d for all cases in the insets of Fig. 4. Interestingly, for all phase boundaries the central charge as a function of λ_d exhibits exactly an opposite behavior as compared to the EE in terms of decreasing or increasing nature. It seems that these two behaviors contradict each other, i.e., when EE decreases with λ_d, central charge increases. However,

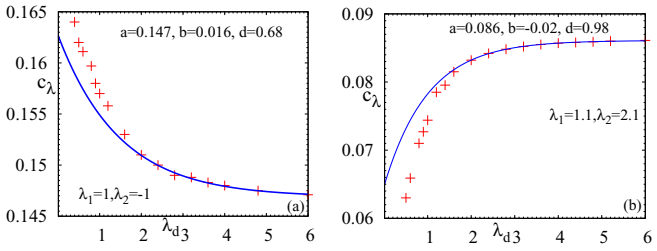

FIG. 5. (a) and (b) show the variation of c_λ with λ_d as shown in Figs. 4(a) and 4(d), respectively. Here, it has been seen that both the plots can be fitted with $c_\lambda = a + b\exp(-d\lambda_d)$ for $\lambda_d > \lambda_d^u$ as shown by blue solid lines. It indeed indicates that the effective central charge eventually saturates for strong impurity limit with an exponential damping. The values of fitting parameters are provided inside the plots.

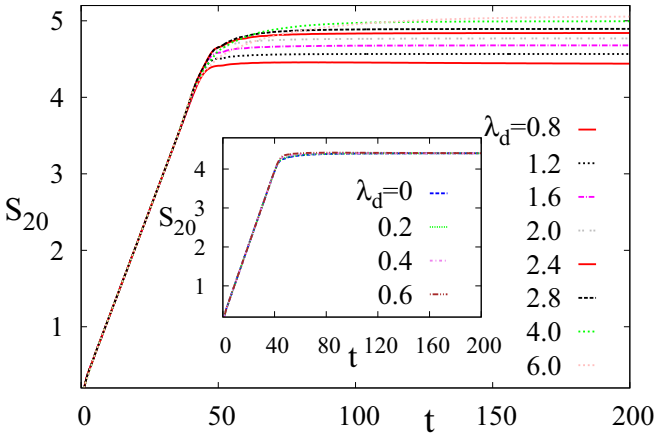

FIG. 6. Evolution of the EE as a function of time for different values of the impurity strength (λ_d). It can be observed that the EE gets affected by the λ_d after a certain value of λ_d when the system is quenched to $n = 0{-}n = 1$ phase boundary (with $\lambda_1 = 1$ and $\lambda_2 = 0$) from $n = 0$ phase with $\lambda_1 = 0.5$. The different curves from bottom to top are given by, solid red line ($\lambda_d = 0.8$), dashed black line ($\lambda_d = 1.2$), long-dashed-dotted pink line ($\lambda_d = 1.6$), double-dotted gray line ($\lambda_d = 2.0$), dashed red line ($\lambda_d = 2.4$), long-dashed black line ($\lambda_d = 2.8$), dashed green line ($\lambda_d = 4.0$), dashed orange line ($\lambda_d = 6.0$). Inset: Shows that saturation value of the EE is almost independent λ_d upto some value, say λ_d^*. At the same time, main plot depicts that the saturation value of the EE increases logarithmically with λ_d after λ_d^*. Here, block length, $l = 20$ and $N = 300$.

this is indeed easy to explain using γ_λ, which also changes with λ_d in an opposite way compared to c_λ.

Let us now extensively investigate the behavior of central charge as reflected in c_λ with λ_d. A clean spin chain (i.e., with $\lambda_d = 0$) with open boundary condition in one dimension has the central charge $c = 1/2$ and 1 (with $c_0 = 1/12$ and $c_0 = 1/6$) for Ising and anisotropic critical lines respectively. We note that for Figs. 4(b), 4(c) and 4(d) with $\lambda_d = 0$, c_0 close to $1/12$, which correspond to Ising critical line, whereas for Fig. 4(a), $c_0 \sim 0.161$, which represents the anisotropic critical line.

For the phase boundaries separating $n = 2$ phase from others [see inset of Figs. 4(a), 4(c) and 4(d)], a careful analysis suggests that effective central charge contained in c_λ that follows the relation: $c_\lambda \approx \alpha\log(\lambda_d) + \beta$ for a range $\lambda_d^l < \lambda_d < \lambda_d^u$, where the values of λ_d^l and λ_d^u depend on the strengths of λ_1 and λ_2. Afterwards, it eventually saturates with an additional exponential damping term given by $\exp(-\lambda_d)$ (see Fig. 5). The saturation characteristics of c_λ for strong impurity limit can be explained by the mathematical form given by $c_\lambda = a + b\exp(-d\lambda_d)$; hence $\lambda_d \to \infty$, $c_\lambda \to a$.

In contrast, on the $n = 1 - n = 0$ phase boundary (with $\lambda_2 = 0$) the effective central charge shows a linear relation with λ_d, $c_\lambda = \beta + \alpha\lambda_d$. Interestingly, in this case, the value of β is close to $c_0 = 1/12$, which is the central charge on that boundary with $\lambda_d = 0$. Therefore, the term $\alpha\lambda_d$ can be considered as the correction over the bare central charge due to the application of the impurity. It is noteworthy that over the complete phase boundary with $\lambda_2 \neq 0$ and even in the strong impurity limit this linear behavior remains unaffected. Hence it can be inferred that the impurity term indeed plays a distinctly different role in the phase boundaries shared with $n = 2$ phase compared to others.

In this connection, we would like to mention that for a disordered quantum spin chain, an effective central charge comes into play instead of the bare central charge obtained in the clean limit [20]. We here show that even a single impurity term can also lead to an effective central charge. At the same time, this effective central charge has distinct scaling relations with the strength of the impurity over different phase boundaries.

B. Nonequilibrium

In the previous section, we have discussed the influence of the impurity term on both critical and off-critical EE when the system is in equilibrium. Provided the general formalism for calculating the time evolution of the EE with a complex term in the Hamiltonian in Eq. (3) as presented in Sec. III, here we will now investigate the effect of the impurity term $H_{\rm imp} = -i\lambda_d a_1 a_2$ on the evolution of the EE when the Majorana chain is suddenly quenched to various critical points.

Let us first assume a situation where λ_1 is suddenly changed from $n = 0$ phase to $n = 1 - n = 0$ phase boundary by fixing λ_2 at 0. The EE after the sudden quench increases linearly up to a time $t^* = l/v$ where v is the group velocity of the quasiparticles generated due to the sudden quench (see Fig. 6) and l being the length of subsystem. This phenomena has been explained in the earlier related literature using the picture of quasiparticle propagation through the system after the quench [19]. We find that the group velocity v, numerically calculated from the final real-space Hamiltonian, is almost independent of λ_d and it remains at nearly equal to 0.5 in this case. This also can be observed from Fig. 6 where the EE for a block of length $l = 20$ shows a linear rise with time up to $t^* \simeq 40$ with different values of λ_d. After time $t = t^*$, the EE saturates at some finite values that depend on the strength of λ_d. The inset of Fig. 6 shows that the EE curves almost overlap with each other even in the saturation region up to a threshold value of λ_d, denoted by λ_d^*. At the same time, for $\lambda_d > \lambda_d^*$, the saturation value increases with λ_d. It has been observed from the plot that the value of λ_d^* depends only on the final values of parameters λ_1 and λ_2.

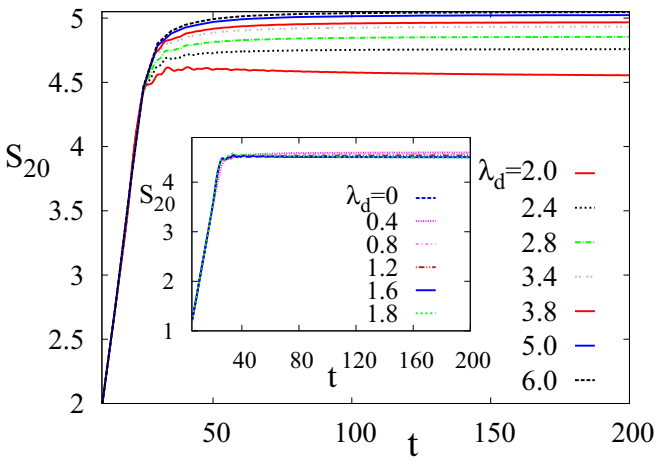

FIG. 7. Variation of the EE with time after quenching the system to $n = 0{-}n = 2$ boundary ($\lambda_1 = 1$ and $\lambda_2 = -1$) from $n = 0$ phase with $\lambda_2 = -0.5$ and $\lambda_1 = 1$. The various curves from bottom to top are given as solid red line ($\lambda_d = 2.0$), dashed black line ($\lambda_d = 2.4$), long-dashed-dotted green line ($\lambda_d = 2.8$), double-dotted gray line ($\lambda_d = 3.4$), dashed red line ($\lambda_d = 3.8$), solid blue line ($\lambda_d = 5.0$), long-dashed black line ($\lambda_d = 6.0$). Here, block length, $l = 20$ and $N = 300$. Inset plot shows that saturation value of the EE is weakly dependent on λ_d and decreases by a small amount with increasing the value of λ_d up to a certain value, say λ_d^*. On the other hand, the main plot depicts that the saturation value of EE increases with λ_d in a nonlinear fashion after λ_d^*.

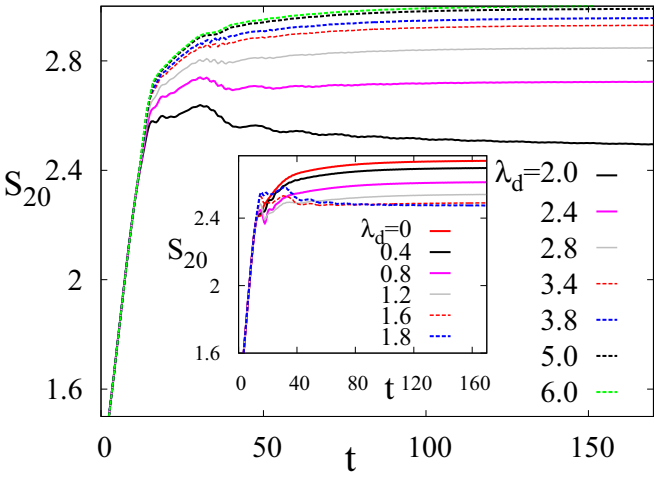

FIG. 8. Time evolution of the EE is affected by the impurity strength as the system is quenched to $n = 1{-}n = 2$ boundary (with $\lambda_1 = 1$ and $\lambda_2 = 2$) from $n = 2$ phase with $\lambda_1 = 0.5$ and $\lambda_2 = 2$. The different curves from bottom to top are denoted by solid black line ($\lambda_d = 2.0$), solid pink line ($\lambda_d = 2.4$), solid gray line ($\lambda_d = 2.8$), long-dashed red line ($\lambda_d = 3.4$), long-dashed blue line ($\lambda_d = 3.8$), long-dashed black line ($\lambda_d = 5.0$), long-dashed green line ($\lambda_d = 6.0$). Here, block length, $l = 20$ and $N = 300$. Inset: It can be seen that the saturation value of the EE decreases slowly when λ_d increases up to a certain value λ_d^*. Main plot: Similar to the previous cases, after λ_d^*, the saturation value of the EE increases with λ_d in a nonlinear fashion.

One can see from Fig. 7 that the linear behavior of the EE persists up to $t = l$ for the $n = 0 - n = 2$ boundary as v becomes unity there. In contrast to the previous case, here the saturation value of the EE indeed decreases by a small amount with increasing λ_d when $\lambda_d < \lambda_d^*$. Here also the saturation value of the EE increases with λ_d after $\lambda_d > \lambda_d^*$. On the other hand, the EE increases linearly up to $t = 2l/3$ as $v \simeq 3/2$ over the $n = 2 - n = 1$ phase boundary (see the Fig. 8). In this case, the decrease of the saturation value of the EE with increasing λ_d (up to λ_d^*) is more prominent than the $n = 0 - n = 2$ boundary. However, the behavior of the EE for $\lambda_d > \lambda_d^*$ seems to be similar to the previous cases.

We are now interested to determine the relation between the saturation value of the EE and λ_d. It can be observed from Fig. 9 that the variation of the saturation value of EE with λ_d ($> \lambda_d^*$) is given by $S_{\rm sat} \propto \log \lambda_d$ for all three cases discussed above. The logarithmic behavior of EE suggests the fact that λ_d affects the EE in an identical manner irrespective of the nature of the phase boundary, i.e., whether the phase boundary separates a topological phase from a nontopological phase or two different topological phases. The semiclassical theory of the EE [73] suggests that the more number of quasiparticles is generated as one increases the strength of impurity and as a result saturation value of the EE increases with λ_d. However, the logarithmic dependence of saturation value of EE for $\lambda_d > \lambda_d^*$ can not be explained by this theory of quasiparticle generation.

Similar to the variation of c_λ on the phase boundary shared with $n = 2$ phase as shown in Fig. 5, we find that the saturation value of EE eventually approaches to a fixed value with λ_d for strong impurity limit [see Fig. 10(a)]. In contrast to the equilibrium case, the saturation in $S_{\rm sat}$ is also observed for $n = 1{-}n = 0$ boundary [see Fig. 10(b)], whereas c_λ shows linear variation for whole range of λ_d there. The strong impurity limit here is meant to be above the range of λ_d within which logarithmic rise of $S_{\rm sat}$ is observed. As described earlier, it might be the case that after a cutoff value of λ_d the rate of quasiparticle generation decreases with an

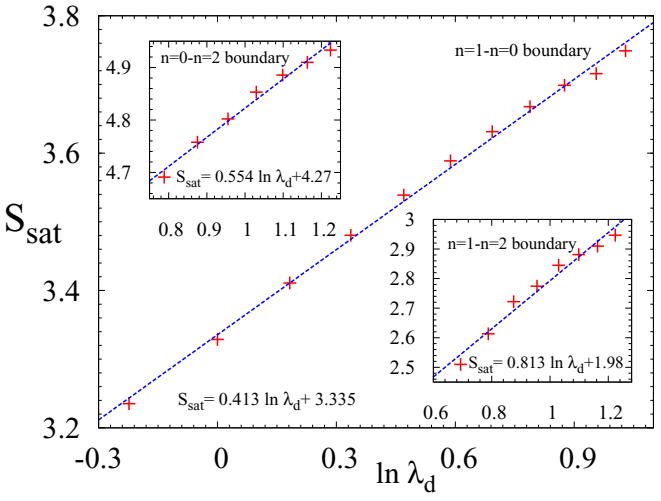

FIG. 9. We have plotted the saturation value of the EE as a function of $\ln \lambda_d$ for three different cases studied in Figs. 6, 7, and 8. This plot shows that saturation value of the EE increases linearly with $\ln \lambda_d$ after λ_d^*. The blue dashed lines represent the fitted curve: $S_{\rm sat} = \alpha \ln \lambda_d + \beta$.

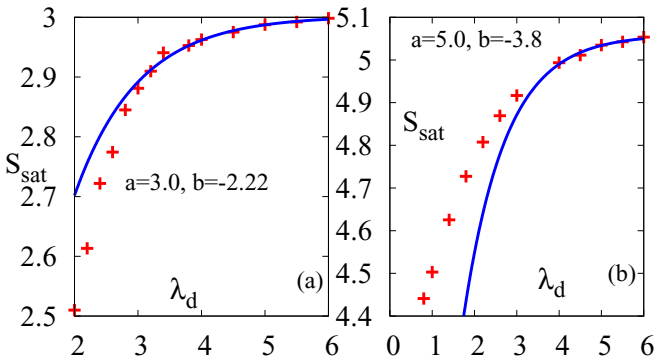

FIG. 10. Variation of S_{sat} as a function of λ_d when the quenching is performed up to (a) $n = 1-n = 2$ and (b) $n = 1-n = 0$ phase boundaries. After a logarithmic increase, S_{sat} follows the relation $c_\lambda = a + b\exp(-\lambda_d)$ (depicted by blue solid lines).

exponential damping factor resulting $S_{sat} = a + b\exp(-\lambda_d)$ for strong impurity limit. It can be noted that the ranges of λ_d within which the logarithmic rise in c_λ and S_{sat} occurs following saturation are different from each other.

For a global quench to a critical point it has been shown that the EE follows the relations $S_l \sim ct$ for $t < l/v$ and $S_l \sim cl$ for $t > l/v$ [32]; therefore, the central charge plays a crucial role in both the temporal regions. In our case, interestingly, the linear rise of EE with t remains almost unaltered even if c_λ (i.e., essentially the effective central charge) depends on λ_d, although, some minor changes occur in a small time window where the linear rise terminates and the saturation starts. On the other hand, saturation values of EE behave in an identical manner as exhibited by c_λ for boundaries shared with $n = 2$ phase. Therefore, the upshot of λ_d on the effective central charge gets imprinted on the saturation characteristics of EE. Considering the complete nonequilibrium evolution over all the phase boundaries, one can say that the outcome of the effective central charge seems to behave differently with λ_d as compared to the static limit.

In the present context, one can easily note the difference between equilibrium and nonequilibrium scenarios. The nonequilibrium case that we consider can be illustrated as two simultaneous quenches comprising of a global and a local quench. The global quench is performed by changing a parameter of the Hamiltonian up to a critical point, whereas addition of an impurity term at one end of the chain can be considered as a local quench. Therefore the behavior of the EE with time is determined by both the quenches unlike the situation to the equilibrium case where one impurity term is added in the critical chain. This might be one of the reasons why the linear rise of the EE with time is not noticeably affected by the impurity term. In other words, for linear rise of the EE global quench dominates and effectively central charge remains unaffected by the impurity term. In addition, this anomalous behavior may be due to the fact that the EE in static limit is governed by low-energy properties of the ground state only, whereas, due to the sudden quench, the behavior of EE in nonequilibrium case is substantially determined by the excited energy levels. In this connection, we would like to mention that the contribution from higher excited state is extensively studied using the spectral function following a sudden quench between two different phases in the Lipkin-Meshkov-Glick model [74].

V. CONCLUSIONS

We investigate the critical characteristics of EE in both equilibrium and nonequilibrium situations by considering the effect of the impurity in a three-spin-interacting model. We show that the topological phase transitions can be detected by the derivative of EE that shows cusps in the vicinity of the phase boundaries. By applying the impurity term we can probe that the edge modes do contribute in the EE. Additionally, our study suggests that the equilibrium EE satisfies a finite-size scaling relation $l^{-1}\ln l$. Interestingly, similar to disordered systems, the application of a single impurity in the system leads to the effective central charge while keeping the critical scaling relation (i.e., $\log l$) of the EE unchanged. For phase boundaries connected with $n = 2$ phase, we find that the effective central charge shows a logarithmic scaling relation with λ_d in a certain range of λ_d following the saturation with an exponentially damping factor at large λ_d. At the same time, the central charge acquires a linear correction as a function of λ_d over the bare value at the phase boundary separating $n = 0$ and $n = 1$ phases.

Furthermore, we extend our study to the time evolution of the EE following the a critical quench where the impurity term is only added to the boundary of the quenched critical chain. In this case, we focus on the effect of the impurity Hamiltonian on the saturation value of the EE as the linear rise remains unaffected. Our study indicates that irrespective of the phase boundaries there exists a threshold value of the impurity strength after which the saturation value of the EE increases logarithmically with impurity strength. The threshold value of the impurity depends on the final parameters of the critical Hamiltonian. In the strong impurity limit, the increase of saturation value of EE with λ_d is suppressed by an exponential damping factor.

It has been observed that the effect of the impurity term shows up differently in the EE under equilibrium and nonequilibrium situations, i.e., change in the effective central charge due to impurity, as probed in the equilibrium analysis of EE, is substantially visible in the later temporal saturation of EE not in the initial rise with time. We provide two probable reasons for this anomalous behavior. One is related to the competitive effects of two simultaneous quenches. The another one is due to the fact that the higher excited energy levels contribute in the dynamics of EE, whereas, equilibrium behavior of EE is completely governed by the ground state. However, in both the equilibrium and nonequilibrium cases, the range of λ_d within which the effects are appreciably visible depends on the phase boundary and the values of the other parameters.

In recent years entanglement entropy serves as an indicator of thermalization and many-body localization. We would like to mention a few comments in that direction. General belief says that the ballistic growth (i.e., linear in time) of EE is a signature of thermalization for nonintegrable systems [75]. Although in our case the impurity term, being quadratic in fermionic operator, is not able to break the integrability of the system, we find a linear rise of EE followed by a saturation. On the other hand, logarithmic growth of EE for the many-body

localized state is clearly distinguished from the dynamical evolution of EE in the thermalized phase [76].

ACKNOWLEDGMENTS

The authors are grateful to Amit Dutta and Bikas K. Chakrabarti for enlightening discussion. T.N. and A.R. thank IIT Kanpur and SINP Kolkata respectively where the initiation of the work was done. T.N. acknowledges Kush Saha for critically reading the manuscript. A.R. acknowledges financial support from the Israeli Science Foundation Grant No. 1542/14.

APPENDIX: ENTANGLEMENT ENTROPY

To calculate the EE in Eq. (1), we first have to determine the reduced density matrix ρ_l. The nonlocal nature of the underlying Jordan-Wigner fermion allows us to construct a $2l \times 2l$ correlation matrix, given by

$$[\Gamma_l^A]_{2l\times 2l} = [W^\dagger]_{2l\times 2N}[\Gamma^B]_{2N\times 2N}[W]_{2N\times 2l}. \tag{A1}$$

The matrix Γ_l^A is a skew-symmetric matrix, which can be represented in the block-diagonal form $\Gamma_l^C = V\Gamma_l^A V^\dagger$ by an orthogonal transformation with V. Then the matrix Γ_l^C can be written as

$$\Gamma_l^C = \bigoplus_{j=1}^{l} \begin{bmatrix} 0 & \eta_j \\ -\eta_j & 0 \end{bmatrix}. \tag{A2}$$

This defines a new set of Majorana fermion operators

$$c_p = \sum_{q=1}^{2l} V_{pq} e_q. \tag{A3}$$

In this basis, the new correlation matrix is given by

$$\langle c_p c_q \rangle = \delta_{pq} + i\left(\Gamma_l^C\right)_{pq}. \tag{A4}$$

Equation (A2) indicates that the c Majorana fermions are correlated when their site indices are separated by 1. We use this fact in our next steps of calculations.

Finally, we express the Majorana fermions in terms of usual complex fermions. We define l fermionic modes from $2l$ Majorana operators

$$f_j = \frac{c_{2j-1} + ic_{2j}}{2}. \tag{A5}$$

By definition the fermionic modes satisfy the relations

$$\langle f_j f_k \rangle = 0, \;\; \langle f_j^\dagger f_k \rangle = \delta_{jk}\frac{1+\eta_j}{2}. \tag{A6}$$

It signifies that there has no correlation among the l fermionic modes. Using this fact the density matrix of the l fermionic modes can be written as a direct product of l uncorrelated modes $\rho_l = \otimes_{n=1}^{l}\varrho_n$ with each ϱ_n having eigenvalues $(1 \pm \eta_n)/2$. Now, from definition of the EE in Eq. (1), it is given by

$$S(l) = -\sum_{n=1}^{l}\left[\left(\frac{1+\eta_n}{2}\right)\log\left(\frac{1+\eta_n}{2}\right) + \left(\frac{1-\eta_n}{2}\right)\log\left(\frac{1-\eta_n}{2}\right)\right]. \tag{A7}$$

[1] S.-J. Gu, Int. J. Mod. Phys. B **24**, 4371 (2010).
[2] H. T. Quan, Z. Song, X. F. Liu, P. Zanardi, and C. P. Sun, Phys. Rev. Lett. **96**, 140604 (2006).
[3] B. Damski, H. T. Quan, and W. H. Zurek, Phys. Rev. A **83**, 062104 (2011).
[4] W. K. Wootters, Qunatum Inf. Comput. **I**, 27 (2001); M. Q. Horodecki, *ibid.* **I**, 3 (2001).
[5] A. Osterloh, L. Amico, G. Falci, and R. Fazio, Nature (London) **416**, 608 (2002); T. J. Osborne and M. A. Nielsen, Phys. Rev. A **66**, 032110 (2002).
[6] H. Ollivier and W. H. Zurek, Phys. Rev. Lett. **88**, 017901 (2001); W. H. Zurek, Rev. Mod. Phys. **75**, 715 (2003).
[7] G. Vidal, J. I. Latorre, E. Rico, and A. Kitaev, Phys. Rev. Lett. **90**, 227902 (2003).
[8] A. Kitaev and C. Laumann, arXiv:0904.2771v1; J. C. Budich, S. Walter, and B. Tranzettel, Phys. Rev. B **85**, 121405(R) (2012); M. J. Scmidt, D. Rainis, and D. Loss, *ibid.* **86**, 085414 (2012); S. Tewari, S. Das Sarma, C. Nayak, C. Zhang, and P. Zoller, Phys. Rev. Lett. **98**, 010506 (2007).
[9] T. Nag, U. Divakaran, and A. Dutta, Phys. Rev. B, **86**, 020401(R) (2012).
[10] R. Sachdeva, T. Nag, A. Agarwal, and A. Dutta, Phys. Rev. B **90**, 045421 (2014).
[11] S. Suzuki, T. Nag, and A. Dutta, Phys. Rev. A **93**, 012112 (2016).
[12] T. Nag, Phys. Rev. E **93**, 062119 (2016).
[13] T. Nag and A. Dutta, Phys. Rev. A **94**, 022316 (2016).
[14] A. Rajak and U. Divakaran, J. Stat. Mech. (2016) 043107.
[15] B. K. Chakrabarti, A. Dutta, and P. Sen, *Quantum Ising Phases and Transitions in Transverse Ising Models* (Springer, Heidelberg, 1996).
[16] S. Sachdev, *Quantum Phase Transitions* (Cambridge University Press, Cambridge, 1999).
[17] A. Polkovnikov, K. Sengupta, A. Silva, and M. Vengalattore, Rev. Mod. Phys. **83**, 863 (2011).
[18] A. Dutta, G. Aeppli, B. K. Chakrabarti, U. Divakaran, T. Rosenbaum, and D. Sen, *Quantum Phase Transitions in Transverse Field Spin Models: From Statistical Physics to Quantum Information* (Cambridge University Press, Cambridge, 2015).
[19] P. Calabrese and J. Cardy, J. Stat. Mech. (2004) P06002.
[20] G. Refael and J. E. Moore, Phys. Rev. B **76**, 024419 (2007).
[21] I. Peschel, J. Phys. A: Math. Gen. **38**, 4327 (2005).
[22] H. Li and F. D. M. Haldane, Phys. Rev. Lett. **101**, 010504 (2008).
[23] H. Yao and X.-L. Qi, Phys. Rev. Lett. **105**, 080501 (2010).
[24] L. Fidkowski, Phys. Rev. Lett. **104**, 130502 (2010).
[25] F. Pollmann, A. M. Turner, E. Berg, and M. Oshikawa, Phys. Rev. B **81**, 064439 (2010).
[26] P. Facchi, U. Marzolino, G. Parisi, S. Pascazio, and A. Scardicchio, Phys. Rev. Lett. **101**, 050502 (2008).
[27] M. Z. Hasan and C. L. Kane, Rev. Mod. Phys. **82**, 3045 (2010).
[28] X.-L. Qi and S.-C. Zhang, Rev. Mod. Phys. **83**, 1057 (2011).

[29] S. Ryu and Y. Hatsugai, Phys. Rev. B **73**, 245115 (2006).
[30] A. Kitaev and J. Preskill, Phys. Rev. Lett. **96**, 110404 (2006); M. Levin and X. G. Wen, *ibid.* **96**, 110405 (2006).
[31] J. Borchmann, A. Farrell, S. Matsuura, and T. Pereg-Barnea, Phys. Rev. B **90**, 235150 (2014); T. P. Oliveira, P. Ribeiro, and P. D. Sacramento, J. Phys.: Condens. Matter **26**, 425702 (2014); J. Borchmann, A. Farrell, and T. Pereg-Barnea, Phys. Rev. B **93**, 125133 (2016).
[32] P. Calabrese and J. Cardy, J. Stat. Mech. (2005) P04010.
[33] V. Eisler and I. Peschel, J. Stat. Mech. (2007) P06005.
[34] P. Calabrese and J. Cardy, J. Stat. Mech. (2007) P10004.
[35] V. Eisler, D. Karevski, T. Platini, and I. Peschel, J. Stat. Mech. (2008) P01023.
[36] F. Igloi, Z. Szatmari, and Y.-C. Lin, Phys. Rev. B **80**, 024405 (2009).
[37] B. Hsu, E. Grosfeld, and E. Fradkin, Phys. Rev. B **80**, 235412 (2009).
[38] J. Cardy, Phys. Rev. Lett. **106**, 150404 (2011).
[39] I. Bloch, J. Dalibard, and W. Zwerger, Rev. Mod. Phys. **80**, 885 (2008).
[40] T. Kinoshita, T. Wenger, and D. S. Weiss, Phys. Rev. Lett. **95**, 190406 (2005).
[41] T. Kinoshita, T. Wenger, and D. S. Weiss, Nature (London) **440**, 900 (2006).
[42] F. Igloi, Z. Szatmari, and Y.-C. Lin, Phys. Rev. B **85**, 094417 (2012).
[43] M.-C. Chung, Y.-H. Jhu, P. Chen, C.-Y. Mou, and X. Wan, arXiv:1401.0433.
[44] M. Cheneau *et al.*, Nature (London) **481**, 484 (2012).
[45] R. Islam *et al.*, Nature (London) **528**, 77 (2015).
[46] A. Kitaev, Phys. Usp. **44**, 131 (2001).
[47] I. C. Fulga, F. Hassler, A. R. Akhmerov, and C. W. J. Beenakker, Phys. Rev. B **83**, 155429 (2011).
[48] J. D. Sau and S. Das Sarma, Nature Commun. **3**, 964 (2012).
[49] R. M. Lutchyn and M. P. A. Fisher, Phys. Rev. B **84**, 214528 (2011).
[50] W. DeGottardi, D. Sen, and S. Vishveshwara, New J. Phys. **13**, 065028 (2011).
[51] W. DeGottardi, D. Sen, and S. Vishveshwara, Phys. Rev. Lett. **110**, 146404 (2013).
[52] M. Thakurathi, A. A. Patel, D. Sen, and A. Dutta, Phys. Rev. B **88**, 155133 (2013).
[53] W. DeGottardi, M. Thakurathi, S. Vishveshwara, and D. Sen, Phys. Rev. B **88**, 165111 (2013).
[54] J. Alicea, Rep. Prog. Phys. **75**, 076501 (2012).
[55] A. Rajak and A. Dutta, Phys. Rev. E **89**, 042125 (2014).
[56] A. Rajak, T. Nag, and A. Dutta, Phys. Rev. E **90**, 042107 (2014).
[57] A. Kopp and S. Chakravarty, Nature Phys. **1**, 53 (2005).
[58] Y. Niu, S. B. Chung, C.-H. Hsu, I. Mandal, S. Raghu, and S. Chakravarty, Phys. Rev. B **85**, 035110 (2012).
[59] A. Rajak and T. Nag, Phys. Rev. E **96**, 022136 (2017).
[60] W. Son, L. Amico, R. Fazio, A. Hamma, S. Pascazio, and V. Vedral, Europhys. Lett. **95**, 50001 (2011).
[61] S. M. Giampaolo and B. C. Hiesmayr, New J. Phys. **16**, 093033 (2014).
[62] B.-e. Friedman, A. Rajak, A. Russomanno, and E. G. D. Torre, arXiv:1708.03400v2.
[63] T. J. G. Apollaro, G. Francica, D. Giuliano, G. Falcone, G. M. Palma, and F. Plastina, Phys. Rev. B **96**, 155145 (2017).
[64] X. Huang and Z. Yang, Solid State Commun. **204**, 28 (2015).
[65] T. Fukuhara *et al.*, Nature Phys. **9**, 235 (2013).
[66] J. I. Latorre, E. Rico, and G. Vidal, Quantum Inf. Comput. **4**, 48 (2004).
[67] S. Sharma and A. Rajak, J. Stat. Mech. (2012) P08005.
[68] A. Rajak and U. Divakaran, J. Stat. Mech. (2014) P04023.
[69] M. S. Sarandy, Phys. Rev. A **80**, 022108 (2009).
[70] R. Dillenschneider, Phys. Rev. B **78**, 224413 (2008).
[71] Y. Wang, T. Gulden, and A. Kamenev, Phys. Rev. B **95**, 075401 (2017).
[72] T. Gulden, M. Janas, Y. Wang, and A. Kamenev, Phys. Rev. Lett. **116**, 026402 (2016).
[73] H. Rieger and F. Igloi, Phys. Rev. B **84**, 165117 (2011).
[74] S. Campbell, Phys. Rev. B **94**, 184403 (2016).
[75] H. Kim and D. A. Huse, Phys. Rev. Lett. **111**, 127205 (2013).
[76] A. Nanduri, H. Kim, and D. A. Huse, Phys. Rev. B **90**, 064201 (2014).